

Intelligent self-powered sensor based on triboelectric nanogenerator for take-off status monitoring in the sport of triple-jumping

Jiahui Xu^{1,2}, Xuelian Wei^{1,2}, Ruonan Li³, Yapeng Shi^{1,2}, Yating Peng¹, Zhiyi Wu^{1,2,4} (✉), and Zhong Lin Wang^{1,2,4,5} (✉)

¹ Beijing Institute of Nanoenergy and Nanosystems, Chinese Academy of Sciences, Beijing 101400, China

² College of Nanoscience and Technology, University of Chinese Academy of Science, Beijing 100049, China

³ School of Chemistry and Chemical Engineering, Guangxi University, Nanning 530004, China

⁴ CUSTech Institute of Technology, Wenzhou 325024, China

⁵ School of Materials Science and Engineering, Georgia Institute of Technology, Atlanta, GA 30332, USA

© Tsinghua University Press 2022

Received: 11 November 2021 / Revised: 29 January 2022 / Accepted: 8 February 2022

ABSTRACT

In the era of big data and the Internet of Things, the digital information of athletes is particularly significant in sports competitions. Here, an intelligent self-powered take-off board sensor (TBS) based on triboelectric nanogenerator (TENG) with a solid-wooden substrate is provided for precise detection of athletes' take-off status in the sport of triple-jumping, which is sufficient for triple-jumping training judgment with a high accuracy of 1 mm. Meanwhile, a foul alarm system and a distance between the athlete's foot and take-off line (GAP) measurement system are further developed to provide take-off data for athletes and referees. The induced charges are formed by the TBS during taking-off, and then the real-time exercise data is acquired and processed via the test program. This work presents a self-powered sports sensor for intelligent sports monitoring and promotes the application of TENG-based sensors in intelligent sports.

KEYWORDS

self-powered, sports sensor, triboelectric nanogenerator, triple jump, intelligent sports

1 Introduction

In the period of the Internet of Things and big data, people's requirements for intelligent life are increasing gradually [1]. The direct evaluations from signal sensors with high precision are particularly more compelling than artificial judgment in sports events. All aspects of sports activities, such as athletes' performance and physical health [2], can be rapidly collected by intelligent data sensing networks, which can not only accurately evaluate the athlete's performance, but also indicate the elements that influence the athlete's performance, assisting coaches and contestants in developing suitable training plans [3,4]. For example, high-speed cameras and infrared sensors are employed to monitor competition data in the triple jump. However, due to the requirements for additional power supplies with the high cost and negative environmental impact, such as batteries [5–8], it is critical to develop self-powered sensors for sports monitoring.

Triboelectric nanogenerator (TENG), as a self-sufficient power source, has been widely applied due to its advantages of low costs, simple structures, easy integration, and high efficiency [9–11], which was developed by Wang and co-workers for effectively harvesting and converting irregular mechanical energy or nano energy into electrical energy [12–14]. By changing different materials, structures, and modes, TENG can be utilized to collect various types of low-frequency and randomly oriented mechanical

energy in the environment [15, 16], such as blue energy [17–21], wind energy [22–27], energy of dripping liquid [28], and other mechanical energies [29–31] for a variety of applications, including energy harvesting [32–35] and self-powered sensors [36–39]. Most notably, TENG-based sensors include smart wearable sensors for human health and exercise state monitoring [40–49] and other sensors for vehicle status monitoring [50], ship status monitoring [51, 52], sports sensing [5, 53, 54], etc.

In recent years, the sensing applications of TENG have become more extensive, which have facilitated many aspects of people's life [35, 50]. Meanwhile, there are many intelligent applications of TENG in the field of sports. Luo et al. utilized the treated wood to design a smart sensor that was applied to a ping-pong table to capture the location of the ball on the table and detect the edge ball [5]. Wu et al. proposed a cylindrical self-powered multifunctional sensor that could be integrated with a boxing glove, realizing the acceleration tracking of the boxer [55]. In spite of these applications, TENG-based sensors still have great potential in intelligent sports and how to monitor and evaluate the data involved in sports in real-time is a crucial research that deserves significant consideration.

Here, a TENG-based self-powered take-off board sensor (TBS) is prepared for monitoring the triple-jumping process, where a

polymer rubber with a similar hardness to the wood is selected as the triboelectric layer which also has good charge transfer and capture capability. The polymer rubber can generate surface charges when contacts with a moving object, which causes an induced potential when the object separates from it. To balance the potential, charges flow across the electrodes inside the rubber, resulting in electrical signals. Then, the electrical signals of TBS could be utilized to assess whether the athletes break the rules. Moreover, a distance between the athlete's foot and take-off line (GAP) measurement system is developed to precisely record the statistics of athletes' taking off conditions with the real-time data processed by mobile phones or computers in daily training. The ingenious design of TBS opens up a new strategy for the fabrication of TENG and provides prosperous applications in the field of intelligent sports.

2 Results and discussion

2.1 Structure and working principle of TBS

In the sport of triple-jumping, there is a take-off line on the front end of the take-off board to determine if the athlete's take-off is foul. In addition to recording the effectiveness of the take-off condition, some equipment is adopted to provide the GAP. Here, an intelligent triple-jumping take-off board is constructed based on a single-electrode mode TENG, which is composed of a slotted solid-wooden board, wires for transferring induced charges, and urethane rubber as triboelectric layers (Fig. 1(a)(a₁)). Figure 1(a) shows the entire process of the triple jump, as well as the function and structure of TBS. A cross-sectional view of the TBS and a depiction of its internal structure are illustrated in Figs. 1(a)(a₂) and 1(a)(a₃), respectively. By converting mechanical energy into electricity, the TBS can sense a moving object in single-electrode mode with the function of timely feedback on the GAP value which means the take-off position. As depicted in Fig. 1(a)(a₄), the first line marked blue is the take-off line, and the GAP value corresponding to the athlete's foot position is 3 cm.

To describe the working principle of TBS in detail, a nitrile rubber strip with a width of 9 mm is used to better explain the

generation process of the electrical signal, which is presented in Fig. 1(b). Urethane rubber tends to gain negative charges due to its higher capacity to receive electrons. Hence, the rubber strip will release electrons when it comes into touch with urethane rubber, leaving the urethane rubber negatively charged. Since the separation between the two surfaces expands as the rubber strip moves away, the triboelectric charges cannot be transferred or neutralized for a time. Then, a little quality of positive charges will flow from the ground to the wire electrodes embedded in the urethane rubber to neutralize the charges. When the rubber strip is approaching back to the urethane rubber, the electrons will be transferred back to the electrode, causing the gradual decrease of positive charges in the wire. The simulated potential distribution by finite-element analysis (COMSOL Multiphysics) is referred in Figs. 1(c)(c₁)–1(c)(c₄) to demonstrate the potential changes between two triboelectric layers in different phases, demonstrating that the TBS can be applied as a self-powered sports sensor by generating the change of electrical signals.

2.2 Electrical characterizations for the TBS

The wires with small diameters and good toughness are used as the electrodes of TBS in the basic performance tests. The impact of a linear motor is employed in the experiment to simulate the take-off movement in the triple jump. Figures 2(a)–2(c) demonstrate the open-circuit voltage (V_{oc}), transfer charge quantity (Q_{sc}), and short-circuit current (I_{sc}) of TBS under the simulated acceleration of 1 m/s^2 during the contact-separation process. Apparently, the V_{oc} , Q_{sc} and I_{sc} reach 1.3 V, 0.5 nC, and 8.4 nA in each cycle, respectively. These electrical signal variations can be effectively transmitted by the TBS. Subsequently, the change of voltage is selected as the judgment signal of the intelligent sensor.

As depicted in Fig. 2(d), a durability test is performed to determine the TBS's output stability. After 5,000 cycles of continuous operation at 1 Hz, the output voltage of the TBS remains about 1.5 V, indicating that the sensor has a long service life that satisfies the needs of daily use. In addition, a multi-channel signal interference test is performed to evaluate the effectiveness of the TBS's signal. As illustrated in Fig. 2(e), the output voltage signals are obtained from the multi-channel

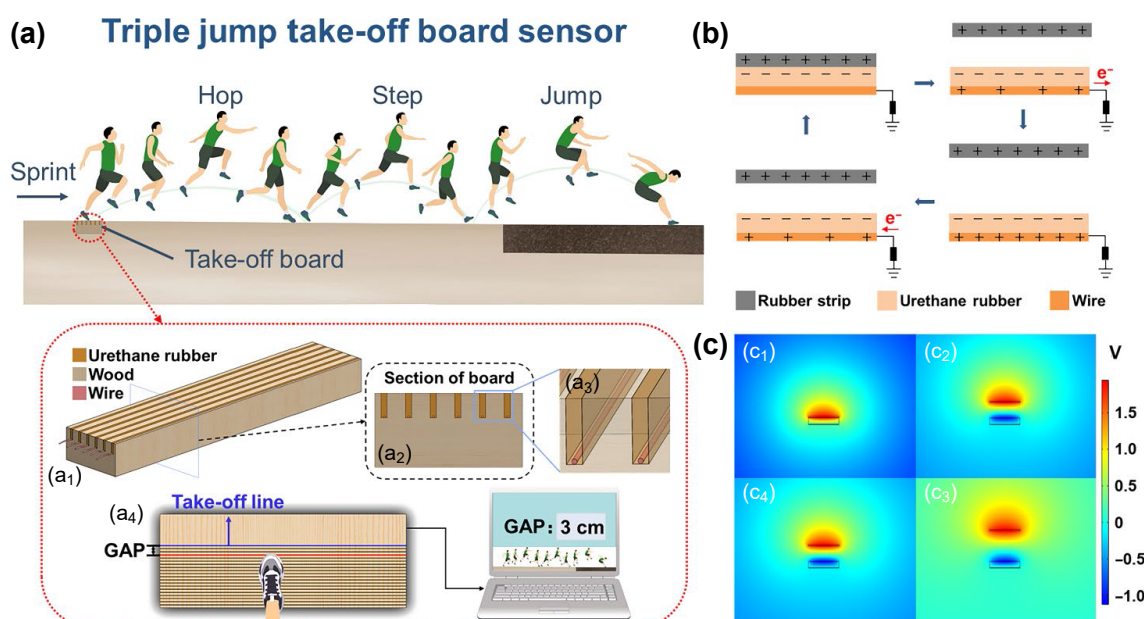


Figure 1 Application, structure, and working mechanism of the TBS. (a) Schematic diagram of application scenarios and structure of TBS. (a₁) Schematic illustration of the designed structure of TBS. (a₂) Cross-sectional view of TBS. (a₃) Transparent view of TBS structure. (a₄) Application of TBS. When the athlete steps on the TBS, the computer interface gives the corresponding GAP value of 3 cm. (b) Operating principle of the TBS in single-electrode mode. (c) The potential distribution of TBS simulated by COMSOL Multiphysics. (c₁)–(c₄) The potential changes of the two triboelectric layers during the contact–separation process.

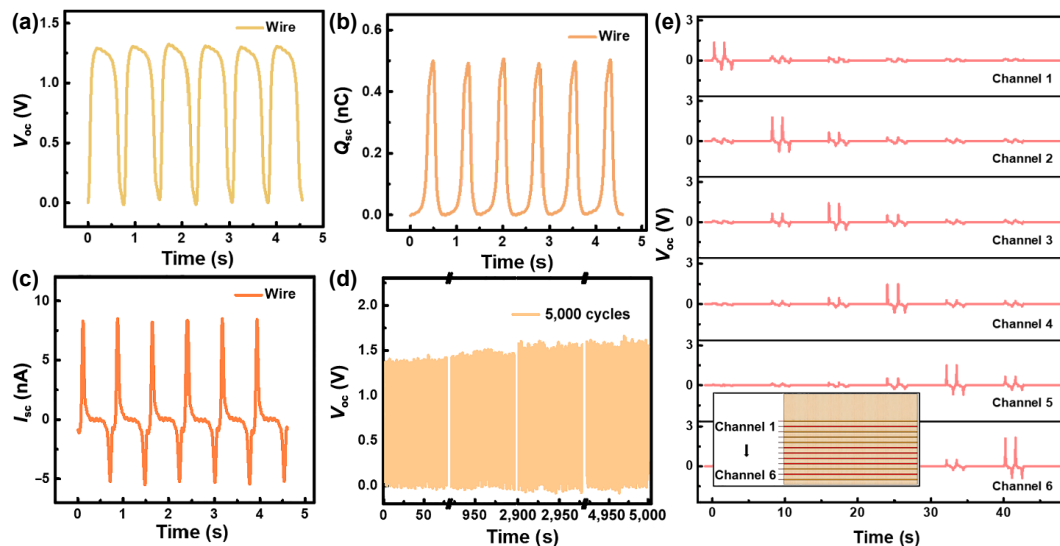


Figure 2 The basic output performance of TBS with wires as electrodes. (a)–(c) V_{oc} , Q_{sc} , and I_{sc} of the TBS. (d) Schematic illustration of durability test of TBS. (e) Schematic diagram of each channel's output voltage and position in the multi-channel signal interference test, and the voltage signal of each channel is shown in two contact–separation cycles.

acquisition card by contacting and separating the nitrile rubber strip with six channels in sequence for two cycles. Notably, when the rubber strip contacts one channel, the voltage signals generated from other channels can be noticed. The reason for the crosstalk signal is that when the rubber strip separates from the urethane rubber after the contact process, a new electric field is formed, resulting in an induced charge on the electrode in the adjacent channel. Moreover, the voltage at the contact position ranges from 2.4 to 3.0 V and the crosstalk signal is small, which is less than half of the contact signal. The influence of the crosstalk signal can be solved in the subsequent programming. Accordingly, the contact channel between the rubber strip and TBS can be easily identified by the voltage signal to fulfill the goal of determining location.

To explore the sensor's universal production and select optimal electrode material, several conductive wires typically used in the textile industry and a kind of multicore cable are chosen as the electrodes of the TBS (Fig. S1 in the Electronic Supplementary Material (ESM)). Six varieties of conductive threads are available: a metal sewing thread (MST), two types of Ag fiber sewing threads (SFST) with diameters of 0.15 and 3 mm, and three types of stainless-steel sewing threads (SST) with diameters of 0.15, 0.3, and 0.5 mm, respectively. As illustrated in Fig. 3(a), the output voltages of a series of sensors constructed by different electrodes are detected under the same test conditions. In contrast, the output voltage of the multicore cable is the highest (3.2 V) and the corresponding output performances including I_{sc} and Q_{sc} are shown in Fig. S2 in the ESM. The improved output performance by the multicore cable makes it easier for the test platform to detect the signals. Due to many thin Cu wires integrated into every cable of the multicore cable, the overall electrode area is improved, thus increasing the interfacial area between the triboelectric layer and the electrode, leading to an increase in electrical signals. Furthermore, the multicore cable is also convenient for wiring and organization. Therefore, it is chosen as the electrodes of the TBS in the following measurements.

To measure the accuracy of TBS, the sensitivity of the channel is tested by changing the contact position of the rubber strip and the signals generated by the two channels are detected. As illustrated in Fig. 3(b), the upper end of the rubber strip is firstly flushed with the upper end of channel 2, then the electrical outputs of the two channels are measured and compared as the rubber strip moves up in increments of 2 mm for a total distance of

12 mm. When the rubber strip moves up for a distance of 4 mm, the rubber strip is directly above channel 2 (Fig. S3(a) in the ESM), and the voltage of channel 2 achieves the maximum value (Fig. 3(c)). Since the rubber strip's surface is curved with high medium and low sides, when the rubber strip is directly above channel 2, the triboelectric area between the rubber strip and channel 2 is the largest, causing the greatest voltage signal. Initially, the voltage of channel 1 is at a very low level. With the gradual movement of the rubber strip, the electrical performance of channel 2 decreases, while the voltage of channel 1 increases (Fig. 3(c)). Channel 1 begins to show a strong signal when the rubber strip moves up to 10 mm. At the same time, the rubber strip has just left channel 2 and the distance from the rubber strip to channel 2 is 1 mm (Fig. S3(b) in the ESM). The voltages of channels 1 and 2 are 1.3 and 0.5 V, respectively. The difference in signals between the two channels can be used to determine the effective contact position. It is concluded that the sensing sensitivity of the sensor can achieve 1 mm, and such high sensitivity of TBS can fulfill the demands of judgment in triple-jumping training.

Additionally, the distance between the electrode and the surface of the triboelectric layer can be adjusted to achieve the transverse position judgment. Here, the electrode is placed obliquely, where its two ends are fixed to the top of the left end and the bottom of the right end of the groove, respectively (Fig. 3(d)(d₁)). In this way, the distance between the electrode and the surface of the urethane rubber continuously rises in the TBS. The output voltages are 2.8, 1.9, and 1.4 V when the distances between the test position and contact position of the rubber strip are set as 6, 26, and 36 cm, respectively (Figs. 3(d)(d₂) and 3(e)), while the corresponding heights between the electrode and the surface of urethane rubber are 0.96, 4.15, and 5.75 mm, respectively (Fig. S4 in the ESM). The difference between these voltages can be used to estimate the moving object's contact position with the TBS. It is proved that this method can be used to determine the contact position in the horizontal scale because of the relationship between positions and voltages. To demonstrate the practicality of TBS in practical application, three sneakers made of various materials are utilized to impact the TBS and the corresponding output voltages of different sneakers are graphically illustrated in Fig. 3(f). All the sports shoes made of different materials can produce discernible electrical outputs: The shoe made of sticky rubber & ethylene vinyl acetate (EVA) rubber generates the highest voltage around 45 V, the natural rubber shoe has the lowest output voltage of 15 V, and

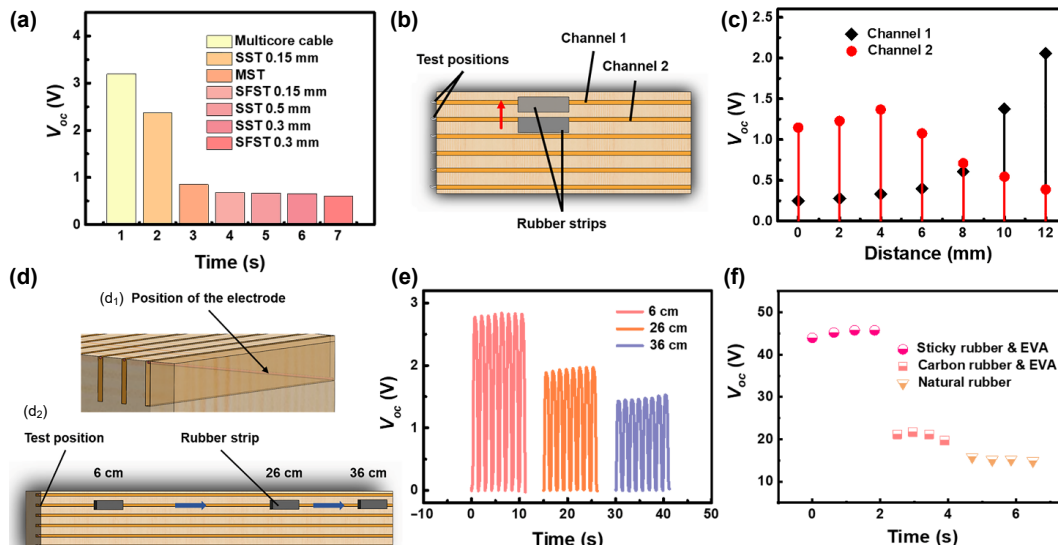


Figure 3 Electrode material, accuracy, structure optimization, and practical test of TBS. (a) Comparison of output voltages of electrodes with different materials under the same conditions. (b) Schematic diagram of the rubber strip's position in the accuracy test. (c) The relationship between the two channels' output voltages and the rubber strip's upward movement distance. (d) Performance test of the TBS when the electrodes are diagonally placed. (d₁) Transparency diagram of the diagonally placed electrode. (d₂) Positions of the rubber strip. (e) Comparison of voltages at different positions from the test terminal. (f) Output voltages of TBS when shoes with different materials stepping on it.

the output voltage of C rubber & EVA shoe is 20 V, which demonstrates that the TBS has universal applicability as a sensor in the sport of triple-jumping without equipping with special shoes for the TBS.

2.3 Application of the TBS

One of the most essential functions of the take-off board in the triple jump is to determine the validity of an athlete's performance based on the take-off line. In official competitions, this judgment is mainly based on high-speed cameras and referees, whereas the TBS can be used to provide a precise foul assessment at a lower cost. The application scenario and physical photo of TBS are shown in Fig. 4(a). Moreover, a matching test system based on the TBS is constructed to obtain the real-time data efficiently with high quality. A signal processing equipment (SPE) is composed of a microprogram control unit, a bluetooth transmitter, and a battery, as plotted in Fig. 4(b)(b₁). The TBS is combined with the SPE to form a foul alarm system (Fig. S5(a) in the ESM), where the multicore cable is used as the electrodes. Meanwhile, a program on a mobile phone can receive signals from SPE and make violation judgments.

Figures 4(b)(b₂) and 4(b)(b₃) demonstrate the relevant results displayed by a mobile phone when an athlete takes off foul or correctly, respectively. Firstly, the mechanical movement can be transformed into an electrical signal and synchronously transferred by TBS when the athlete steps on the take-off line. Secondly, the SPE can detect the electrical signal and judge it as "1". Thirdly, as shown in Fig. 4(b)(b₂), the real-time judgment can be processed and displayed by a mobile phone as "OUT", followed by a sound to indicate that the jump is invalid. Contrarily, the voltage signal can be assessed as "0" when the athlete steps the correct position of the TBS, then the judgment is shown as "PASSED" on the mobile phone, with a voice prompting that the jump is effective (Fig. 4(b)(b₃)). Photographs of the foul alarm system's relevant interfaces of these conditions are included in Figs. S6(a)(a₁) and S6(a)(a₂) in the ESM. Two triple-jumping states can be judged accurately in real-time with such an alarm system (Movie ESM1). The monitoring of take-off status can be accomplished with high accuracy, low cost, and timely feedback using simple programming and a bluetooth transceiver. The foul alarm system can be utilized not only in competitions but

also in athletes' daily trainings. Without the help of others, athletes can acquire whether the jump is successful during training, which is more convenient and intelligent.

In addition to the foul alarm system, the TBS can also be used to obtain the value of the GAP when athletes pedal. When an athlete takes off, the GAP value refers to the distance between the shoe and the take-off line, which is not counted in the total score. However, a larger GAP value during the pedaling process means that the athlete's effective score will be lower than the actual jump distance. Therefore, achieving a smaller GAP value during the competition is a crucial challenge for athletes. Benefiting from the superior output performance, the TBS is also used to build a GAP measurement system. Here, a data acquisition card is adopted to connect the TBS with 20 channels that represent the GAP value from 0 to 19 cm. During the pedaling process, the shoe commonly contacts many channels, the GAP value will be recorded if two conditions are met. One is that it generates an effective voltage, and the other is that it is the closest channel to the take-off line. When the GAP is 0 cm, it indicates that the athlete steps on the take-off line, and the jump is considered foul. The overall picture of the GAP value test is shown in Fig. 4(c)(c₁). When stepping on the TBS, signal changes are collected by a 32-bit NI DAQ device (Fig. S4(b) in the ESM). The real-time data can be shown on a program, after being transmitted to a computer for identification. When an athlete steps randomly on a position of TBS (Fig. 4(c)(c₂)), the corresponding interface of the program is illustrated in Fig. 4(c)(c₃). Furthermore, the GAP value shown in the program is 16 cm. Figure 4(c)(c₄) is a partially enlarged view of the program. Figure S5(b) in the ESM shows the interface of the program, including a cloud image of voltage distribution, real-time GAP value, occurrence time (Fig. 4(c)(c₄)), and a statistics distribution chart that depicts the relationship between the number of pedaling and the GAP value distribution (Fig. 4(c)(c₅)). Each jump can result in a corresponding update in all of the program's items. In addition, when sliding friction occurs, the time associated with the signal can be used to identify the precise position of the taking-off. The test results reveal that the GAP measurement system performs excellently in the sensing accuracy of the take-off position and statistical distribution (Movie ESM2). Furthermore, the statistical distribution chart can be utilized for cloud computing to study the athlete's take-off characteristics, which can help coaches and athletes develop appropriate training plans.

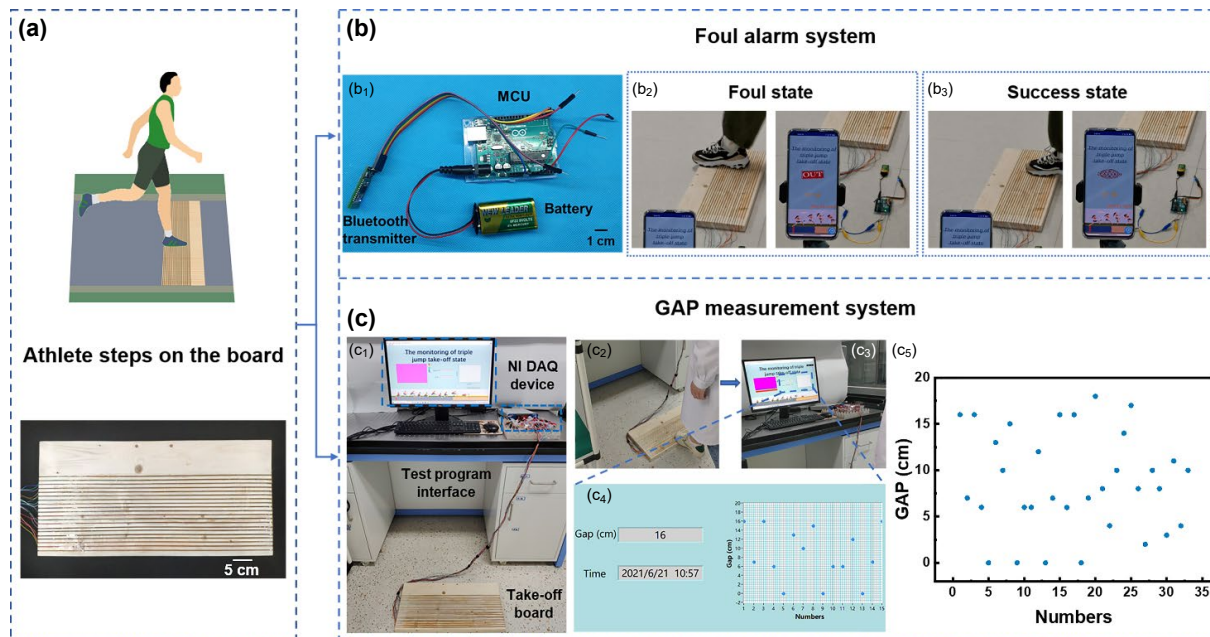


Figure 4 Applications of TBS in foul alarm system and GAP measurement system. (a) Application scenario and physical photo of TBS with multicore cable as electrodes. (b) Application of TBS in foul alarm system. (b₁) Optical photo of SPE. (b₂) When an athlete fouls, the interface of the mobile application displays “OUT”. (b₃) When the athlete takes off correctly, the interface of the application displays “PASSED”. (c) Application of TBS in the GAP measurement system. (c₁) Optical photo of the application scenario of the GAP measurement system. (c₂) and (c₃) The corresponding GAP value is displayed on the computer interface when stepping on TBS. (c₄) Partially enlarged view of the computer interface, including GAP value, time, and a statistical distribution diagram. (c₅) The statistical distribution diagram of the relationship between the number of pedaling and the GAP value distribution.

To further investigate whether the athlete’s weight affects the sensing accuracy of TBS, four experimenters with different weights from 48 to 80 kg (weight range of common triple jumper) are invited to participate in this study, and the voltage comparison results between the adjacent channel and the pedaling channel are shown in Fig. S7 in the ESM. Definitely, the voltage of these adjacent channels is very low, rarely exceeding 1 V, while the voltages of the contacted channel measured by different experimenters are 3.0, 3.1, 3.2, and 3.4 V, respectively. It turns out that TBS is able to play a stable sensing role in a certain weight range of athletes. The combination of function, intelligence, and self-powered supply is achieved by building TENG on a wooden substrate, demonstrating the potential applications of TENG in constructing self-sufficient intelligent sports equipment.

3 Conclusions

In summary, a high-sensitivity and intelligent TENG based on a wooden substrate is developed, which may be employed for self-powered sensing in smart sports as well as big data analysis in the triple jump. With corresponding programs, the TBS can accurately detect the pedal position, evaluate the GAP value of the triple jump, and provide a violation judgment. In addition, the precision of the TBS is up to 1 mm. The training data recorded in real-time can be used for big data analysis to provide athletes with accurate training evaluations and assist coaches in optimizing training methods. This study shows that TENG can be effectively integrated with sports equipment to accurately monitor real-time data while reducing expenses, and it can also expand the application of self-powered sensors in intelligent sports.

4 Experimental section

4.1 Fabrication of the simulation board

There were 19 grooves (60.0 cm × 2.0 mm × 1.0 cm) cut out with a 10-inch table saw on a solid-wooden board (60.0 cm × 20.0 cm

× 3.0 cm). Subsequently, 19 Cu wires were inserted into the grooves respectively, and the ends of each wire were fixed. The base and cure of the liquid urethane rubber (Smooth-on PMC-790) were mixed and stirred evenly at a ratio of 2:1. Furthermore, the mixture was poured into those grooves. After standing for 6 h, the surface was polished and the excess rubber was removed.

4.2 Fabrication of the practical application

The plank used in this part was 60 cm in length, 30 cm in width, and 3 cm in thickness. The same method was adopted as mentioned above to cut out 20 slots (60.0 cm × 2.0 mm × 1.5 cm). And the electrodes were switched to a multicore cable, which was composed of 20 cores.

In addition, the fabrication process for the board required for the application was the same as that for the simulation board described above.

4.3 Characterization and measurements

The rubber strip was driven by a linear motor (LinMot E1200, Switzerland), and basic outputs of TBS were measured by a programmable electrometer (Keithley model 6514, USA), while the real-time data was collected by a testing program constructed by LabView. The output voltage comparison of the six channels was obtained by a multi-channel data acquisition card (NI USB-6356). A maintenance communications unit (MCU) (Arduino uno r3), a bluetooth transmitter (HC-08), and a mobile phone with software were used in the foul alarm system. The GAP measurement system was detected by another data acquisition card (NI USB-6349), and the test platform was constructed by LabView.

Acknowledgements

This research was supported by the National Natural Science Foundation of China (No. 61503051).

Electronic Supplementary Material: Supplementary material (photographs of different electrodes, electrical outputs with multicore cable as electrodes, positions of the rubber strip in the accuracy test, heights between the electrode and the surface of urethane rubber at different positions, connection ways between TBS and MCU, NI DAQ in two applications, program interfaces in two applications, comparison of adjacent channel voltages with different weights of experimenters, Movie ESM1 demonstrates the judgment of take-off status by the foul alarm system, and Movie ESM2 as a demonstration of acquiring GAP value by the GAP measurement system) is available in the online version of this article at <https://doi.org/10.1007/s12274-022-4218-5>.

References

- [1] Hsiao, Y. C.; Wu, M. H.; Li, S. C. Elevated performance of the smart city-A case study of the IoT by innovation mode. *IEEE Trans. Eng. Manage.* **2021**, *68*, 1461–1475.
- [2] Song, W.; Xu, M. M.; Dolma, Y. C. Design and implementation of beach sports big data analysis system based on computer technology. *J. Coastal Res.* **2019**, 327–331.
- [3] Baerg, A. Big data, sport, and the digital divide: Theorizing how athletes might respond to big data monitoring. *J. Sport Soc. Iss.* **2017**, *41*, 3–20.
- [4] Bai, Z. B.; Bai, X. M. Sports big data: Management, analysis, applications, and challenges. *Complexity* **2021**, 2021, 6676297.
- [5] Luo, J. J.; Wang, Z. M.; Xu, L.; Wang, A. C.; Han, K.; Jiang, T.; Lai, Q. S.; Bai, Y.; Tang, W.; Fan, F. R. et al. Flexible and durable wood-based triboelectric nanogenerators for self-powered sensing in athletic big data analytics. *Nat. Commun.* **2019**, *10*, 5147.
- [6] Sommerville, R.; Shaw-Stewart, J.; Goodship, V.; Rowson, N.; Kendrick, E. A review of physical processes used in the safe recycling of lithium ion batteries. *Sustainable Mater. Technol.* **2020**, *25*, e00197.
- [7] Ali, H.; Khan, H. A.; Pecht, M. G. Circular economy of Li batteries: Technologies and trends. *J. Energy Storage* **2021**, *40*, 102690.
- [8] Bai, Y. C.; Muralidharan, N.; Sun, Y. K.; Passerini, S.; Stanley Whittingham, M.; Belharouak, I. Energy and environmental aspects in recycling lithium-ion batteries: Concept of battery identity global passport. *Mater. Today* **2020**, *41*, 304–315.
- [9] Peng, L.; Hu, L. F.; Fang, X. S. Energy harvesting for nanostructured self-powered photodetectors. *Adv. Funct. Mater.* **2014**, *24*, 2591–2610.
- [10] Leung, S. F.; Ho, K. T.; Kung, P. K.; Hsiao, V. K. S.; Alshareef, H. N.; Wang, Z. L.; He, J. H. A self-powered and flexible organometallic halide perovskite photodetector with very high detectivity. *Adv. Mater.* **2018**, *30*, 1704611.
- [11] Liu, Q.; Wang, X. X.; Song, W. Z.; Qiu, H. J.; Zhang, J.; Fan, Z. Y.; Yu, M.; Long, Y. Z. Wireless single-electrode self-powered piezoelectric sensor for monitoring. *ACS Appl. Mater. Interfaces* **2020**, *12*, 8288–8295.
- [12] Fan, F. R.; Tian, Z. Q.; Wang, Z. L. Flexible triboelectric generator!. *Nano Energy* **2012**, *1*, 328–334.
- [13] Wang, Z. L. Triboelectric nanogenerators as new energy technology and self-powered sensors—Principles, problems and perspectives. *Faraday Discuss.* **2014**, *176*, 447–458.
- [14] Zhu, G.; Peng, B.; Chen, J.; Jing, Q. S.; Wang, Z. L. Triboelectric nanogenerators as a new energy technology: From fundamentals, devices, to applications. *Nano Energy* **2015**, *14*, 126–138.
- [15] Dagdeviren, C.; Li, Z.; Wang, Z. L. Energy harvesting from the animal/human body for self-powered electronics. *Annu. Rev. Biomed. Eng.* **2017**, *19*, 85–108.
- [16] Dzhardimalieva, G. I.; Yadav, B. C.; Lifintseva, T. Y. V.; Uflyand, I. E. Polymer chemistry underpinning materials for triboelectric nanogenerators (TENGs): Recent trends. *Eur. Polym. J.* **2021**, *142*, 110163.
- [17] Cheng, P.; Guo, H. Y.; Wen, Z.; Zhang, C. L.; Yin, X.; Li, X. Y.; Liu, D.; Song, W. X.; Sun, X. H.; Wang, J. et al. Largely enhanced triboelectric nanogenerator for efficient harvesting of water wave energy by soft contacted structure. *Nano Energy* **2019**, *57*, 432–439.
- [18] Feng, Y. W.; Liang, X.; An, J.; Jiang, T.; Wang, Z. L. Soft-contact cylindrical triboelectric-electromagnetic hybrid nanogenerator based on swing structure for ultra-low frequency water wave energy harvesting. *Nano Energy* **2021**, *81*, 105625.
- [19] Wang, J. Y.; Pan, L.; Guo, H. Y.; Zhang, B. B.; Zhang, R. R.; Wu, Z. Y.; Wu, C. S.; Yang, L. J.; Liao, R. J.; Wang, Z. L. Rational structure optimized hybrid nanogenerator for highly efficient water wave energy harvesting. *Adv. Energy Mater.* **2019**, *9*, 1802892.
- [20] Yao, Y. Y.; Jiang, T.; Zhang, L. M.; Chen, X. Y.; Gao, Z. L.; Wang, Z. L. Charging system optimization of triboelectric nanogenerator for water wave energy harvesting and storage. *ACS Appl. Mater. Interfaces* **2016**, *8*, 21398–21406.
- [21] Xu, L.; Jiang, T.; Lin, P.; Shao, J. J.; He, C.; Zhong, W.; Chen, X. Y.; Wang, Z. L. Coupled triboelectric nanogenerator networks for efficient water wave energy harvesting. *ACS Nano* **2018**, *12*, 1849–1858.
- [22] Huang, L. B.; Xu, W.; Bai, G. X.; Wong, M. C.; Yang, Z. B.; Hao, J. H. Wind energy and blue energy harvesting based on magnetic-assisted noncontact triboelectric nanogenerator. *Nano Energy* **2016**, *30*, 36–42.
- [23] Liu, S. M.; Li, X.; Wang, Y. Q.; Yang, Y. F.; Meng, L. X.; Cheng, T. H.; Wang, Z. L. Magnetic switch structured triboelectric nanogenerator for continuous and regular harvesting of wind energy. *Nano Energy* **2021**, *83*, 105851.
- [24] Wang, Q.; Zou, H. X.; Zhao, L. C.; Li, M.; Wei, K. X.; Huang, L. P.; Zhang, W. M. A synergetic hybrid mechanism of piezoelectric and triboelectric for galloping wind energy harvesting. *Appl. Phys. Lett.* **2020**, *117*, 043902.
- [25] Chen, B.; Yang, Y.; Wang, Z. L. Scavenging wind energy by triboelectric nanogenerators. *Adv. Energy Mater.* **2018**, *8*, 1702649.
- [26] Bian, Y. X.; Jiang, T.; Xiao, T. X.; Gong, W. P.; Cao, X.; Wang, Z. N.; Wang, Z. L. Triboelectric nanogenerator tree for harvesting wind energy and illuminating in subway tunnel. *Adv. Mater. Technol.* **2018**, *3*, 1700317.
- [27] Quan, Z. C.; Han, C. B.; Jiang, T.; Wang, Z. L. Robust thin films-based triboelectric nanogenerator arrays for harvesting bidirectional wind energy. *Adv. Energy Mater.* **2016**, *6*, 1501799.
- [28] Zhong, W.; Xu, L.; Zhan, F.; Wang, H. M.; Wang, F.; Wang, Z. L. Dripping channel based liquid triboelectric nanogenerators for energy harvesting and sensing. *ACS Nano* **2020**, *14*, 10510–10517.
- [29] Wang, J.; Li, S. M.; Yi, F.; Zi, Y. L.; Lin, J.; Wang, X. F.; Xu, Y. L.; Wang, Z. L. Sustainably powering wearable electronics solely by biomechanical energy. *Nat. Commun.* **2016**, *7*, 12744.
- [30] Gong, W.; Hou, C. Y.; Guo, Y. B.; Zhou, J.; Mu, J. K.; Li, Y. G.; Zhang, Q. H.; Wang, H. Z. A wearable, fibroid, self-powered active kinematic sensor based on stretchable sheath-core structural triboelectric fibers. *Nano Energy* **2017**, *39*, 673–683.
- [31] Wu, H. Z.; Tatarenko, A.; Bichurin, M. I.; Wang, Y. J. A multiferroic module for biomechanical energy harvesting. *Nano Energy* **2021**, *83*, 105777.
- [32] Liu, W. L.; Wang, Z.; Liu, G. L.; Chen, J.; Pu, X. J.; Xi, Y.; Wang, X.; Guo, H. Y.; Hu, C. G. et al. Integrated charge excitation triboelectric nanogenerator. *Nat. Commun.* **2019**, *10*, 1426.
- [33] Guo, H. Y.; Yeh, M. H.; Zi, Y. L.; Wen, Z.; Chen, J.; Liu, G. L.; Hu, C. G.; Wang, Z. L. Ultralight cut-paper-based self-charging power unit for self-powered portable electronic and medical systems. *ACS Nano* **2017**, *11*, 4475–4482.
- [34] Guo, H. Y.; Chen, J.; Wang, L. F.; Wang, A. C.; Li, Y. F.; An, C. H.; He, J. H.; Hu, C. G.; Hsiao, V. K. S.; Wang, Z. L. A highly efficient triboelectric negative air ion generator. *Nat. Sustain.* **2021**, *4*, 147–153.
- [35] Chen, J.; Guo, H. Y.; He, X. M.; Liu, G. L.; Xi, Y.; Shi, H. F.; Hu, C. G. Enhancing performance of triboelectric nanogenerator by filling high dielectric nanoparticles into sponge PDMS film. *ACS Appl. Mater. Interfaces* **2016**, *8*, 736–744.
- [36] Pu, X. J.; Guo, H. Y.; Chen, J.; Wang, X.; Xi, Y.; Hu, C. G.; Wang, Z. L. Eye motion triggered self-powered mechnosensational communication system using triboelectric nanogenerator. *Sci. Adv.* **2017**, *3*, e1700694.

- [37] Guo, H. Y.; Pu, X. J.; Chen, J.; Meng, Y.; Yeh, M. H.; Liu, G. L.; Tang, Q.; Chen, B. D.; Liu, D.; Qi, S. et al. A highly sensitive, self-powered triboelectric auditory sensor for social robotics and hearing aids. *Sci. Robot.* **2018**, *3*, eaat2516.
- [38] Pu, X. J.; Tang, Q.; Chen, W. S.; Huang, Z. Y.; Liu, G. L.; Zeng, Q. X.; Chen, J.; Guo, H. Y.; Xin, L. M.; Hu, C. G. Flexible triboelectric 3D touch pad with unit subdivision structure for effective XY positioning and pressure sensing. *Nano Energy* **2020**, *76*, 105047.
- [39] Qin, K.; Chen, C.; Pu, X. J.; Tang, Q.; He, W. C.; Liu, Y. K.; Zeng, Q. X.; Liu, G. L.; Guo, H. Y.; Hu, C. G. Magnetic array assisted triboelectric nanogenerator sensor for real-time gesture interaction. *Nano-Micro Lett.* **2021**, *13*, 51.
- [40] Huang, P.; Wen, D. L.; Qiu, Y.; Yang, M. H.; Tu, C.; Zhong, H. S.; Zhang, X. S. Textile-based triboelectric nanogenerators for wearable self-powered microsystems. *Micromachines* **2021**, *12*, 158.
- [41] Li, S. M.; Wang, J.; Peng, W. B.; Lin, L.; Zi, Y. L.; Wang, S. H.; Zhang, G.; Wang, Z. L. Sustainable energy source for wearable electronics based on multilayer elastomeric triboelectric nanogenerators. *Adv. Energy Mater.* **2017**, *7*, 1602832.
- [42] Pu, X.; Li, L. X.; Liu, M. M.; Jiang, C. Y.; Du, C. H.; Zhao, Z. F.; Hu, W. G.; Wang, Z. L. Wearable self-charging power textile based on flexible yarn supercapacitors and fabric nanogenerators. *Adv. Mater.* **2016**, *28*, 98–105.
- [43] Seung, W.; Gupta, M. K.; Lee, K. Y.; Shin, K. S.; Lee, J. H.; Kim, T. Y.; Kim, S.; Lin, J. J.; Kim, J. H.; Kim, S. W. Nanopatterned textile-based wearable triboelectric nanogenerator. *ACS Nano* **2015**, *9*, 3501–3509.
- [44] Li, Z.; Zheng, Q.; Wang, Z. L.; Li, Z. Nanogenerator-based self-powered sensors for wearable and implantable electronics. *Research* **2020**, *2020*, 8710686.
- [45] Yu, B.; Yu, H.; Wang, H. Z.; Zhang, Q. H.; Zhu, M. F. High-power triboelectric nanogenerator prepared from electrospun mats with spongy parenchyma-like structure. *Nano Energy* **2017**, *34*, 69–75.
- [46] Kim, K. N.; Chun, J.; Kim, J. W.; Lee, K. Y.; Park, J. U.; Kim, S. W.; Wang, Z. L.; Baik, J. M. Highly stretchable 2D fabrics for wearable triboelectric nanogenerator under harsh environments. *ACS Nano* **2015**, *9*, 6394–6400.
- [47] Zhu, M. L.; Shi, Q. F.; He, T. Y. Y.; Yi, Z. R.; Ma, Y. M.; Yang, B.; Chen, T.; Lee, C. Self-powered and self-functional cotton sock using piezoelectric and triboelectric hybrid mechanism for healthcare and sports monitoring. *ACS Nano* **2019**, *13*, 1940–1952.
- [48] Jiang, Y.; Dong, K.; An, J.; Liang, F.; Yi, J.; Peng, X.; Ning, C.; Ye, C. Y.; Wang, Z. L. UV-protective, self-cleaning, and antibacterial nanofiber-based triboelectric nanogenerators for self-powered human motion monitoring. *ACS Appl. Mater. Interfaces* **2021**, *13*, 11205–11214.
- [49] Li, R. N.; Wei, X. L.; Xu, J. H.; Chen, J. H.; Li, B.; Wu, Z. Y.; Wang, Z. L. Smart wearable sensors based on triboelectric nanogenerator for personal healthcare monitoring. *Micromachines* **2021**, *12*, 352.
- [50] Heo, D.; Kim, T.; Yong, H.; Yoo, K. T.; Lee, S. Sustainable oscillating triboelectric nanogenerator as omnidirectional self-powered impact sensor. *Nano Energy* **2018**, *50*, 1–8.
- [51] Du, T. L.; Zuo, X. S.; Dong, F. Y.; Li, S. Q.; Mtui, A. E.; Zou, Y. J.; Zhang, P.; Zhao, J. H.; Zhang, Y. W.; Sun, P. T. et al. A self-powered and highly accurate vibration sensor based on bouncing-ball triboelectric nanogenerator for intelligent ship machinery monitoring. *Micromachines* **2021**, *12*, 218.
- [52] Zhang, X. Q.; Yu, M.; Ma, Z. R.; Ouyang, H.; Zou, Y.; Zhang, S. L.; Niu, H. K.; Pan, X. X.; Xu, M. Y.; Li, Z. et al. Self-powered distributed water level sensors based on liquid–solid triboelectric nanogenerators for ship draft detecting. *Adv. Funct. Mater.* **2019**, *29*, 1900327.
- [53] Meng, X. S.; Li, H. Y.; Zhu, G.; Wang, Z. L. Fully enclosed bearing-structured self-powered rotation sensor based on electrification at rolling interfaces for multi-tasking motion measurement. *Nano Energy* **2015**, *12*, 606–611.
- [54] Dong, K.; Deng, J. A.; Ding, W. B.; Wang, A. C.; Wang, P. H.; Cheng, C. Y.; Wang, Y. C.; Jin, L. M.; Gu, B. H.; Sun, B. Z. et al. Versatile core–sheath yarn for sustainable biomechanical energy harvesting and real-time human-interactive sensing. *Adv. Energy Mater.* **2018**, *8*, 1801114.
- [55] Wu, Z. Y.; Zhang, B. B.; Zou, H. Y.; Lin, Z. M.; Liu, G. L.; Wang, Z. L. Multifunctional sensor based on translational-rotary triboelectric nanogenerator. *Adv. Energy Mater.* **2019**, *9*, 1901124.